PROCEEDINGS OF SCIENCE

Cosmic Rays in the Orion-Eridanus Superbubble

Théo Joubaud*, **Isabelle A. Grenier, J-M Casandjian**
AIM, CEA, CNRS, Université Paris-Saclay, Université Paris Diderot, Sorbonne Paris Cité, F-91191 Gif-sur-Yvette, France
E-mail: theo.joubaud@cea.fr

The Orion-Eridanus superbubble, formed by the supernovae and supersonic winds of massive stars in the Orion OB associations, has likely fostered cosmic-ray production. The large level of magnetohydrodynamic turbulence in the bubble can also locally alter the diffusion of cosmic rays in space and in momentum. We have studied the cosmic-ray spectrum inside the superbubble by measuring the γ-ray emissivity of gas clouds located in the bubble and along its rim. We have compared these spectra with the average found in other clouds in the solar neighbourhood. To this aim, we have used ten years of data from the *Fermi* Large Area Telescope (LAT) between 250 MeV and 63 GeV. We have modelled the γ radiation from hadronic interactions using multi-wavelength tracers for the hydrogen column densities in the different gas phases, and using the gas distribution in space and velocity to separate the superbubble medium from its foregrounds and backgrounds. The model includes other ancillary components such as inverse-Compton emission, point sources, and solar and lunar emissions. Despite the stellar activity in the superbubble, we find the gas emissivity spectrum to be consistent with the average spectrum measured in the local interstellar medium (ISM). Yet, a small cirrus cloud lying just outside the superbubble exhibits a significantly lower cosmic-ray flux. We will discuss this change in the light of the magnetic-field geometry inferred from the Planck data on dust polarisation.

36th International Cosmic Ray Conference -ICRC2019-
July 24th - August 1st, 2019
Madison, WI, U.S.A.

*Speaker.

PoS(ICRC2019)568

1. Introduction

The Orion-Eridanus superbubble is the nearest site of active high-mass star formation. Located on the far side of the Gould's Belt, it has been the subject of many studies to understand the relationship between stars and interstellar gas such as star formation in a giant molecular cloud, cloud destruction by newly formed stars, and molecular cloud formation. This superbubble has formed from the supernova explosions of the most massive members of the Orion OB associations, at a rate of about one per Myr over the past 12 Myr [1, 20]. Together with the winds of massive stars, these explosions have created an approximately 150 by 300 pc elongated cavity [15] of low-density, high-pressure gas, with a mix of temperatures in the 0.5 to 5 MK range [11]. The slow expansion speed close to 20 km/s and the compression of the swept-up gas behind the outer shock wave has formed a dense outer shell, the near wall of which may be as close as 180 pc from the Sun [1, 11]. The combination of ionising radiation, supersonic stellar winds, and supernovae maintains a turbulent medium in the bubble. Its effect on cosmic rays is to be determined.

2. Gas and dust data

We have analysed the Eridanus part of the superbubble which extends from 43° to 78° in right ascension and from -29° to 21° in declination, as shown in Fig. 1. This region and its perimeter have been chosen to avoid complex gas distributions behind the superbubble. All maps have been projected onto the same 0.25°-spaced Cartesian grid.

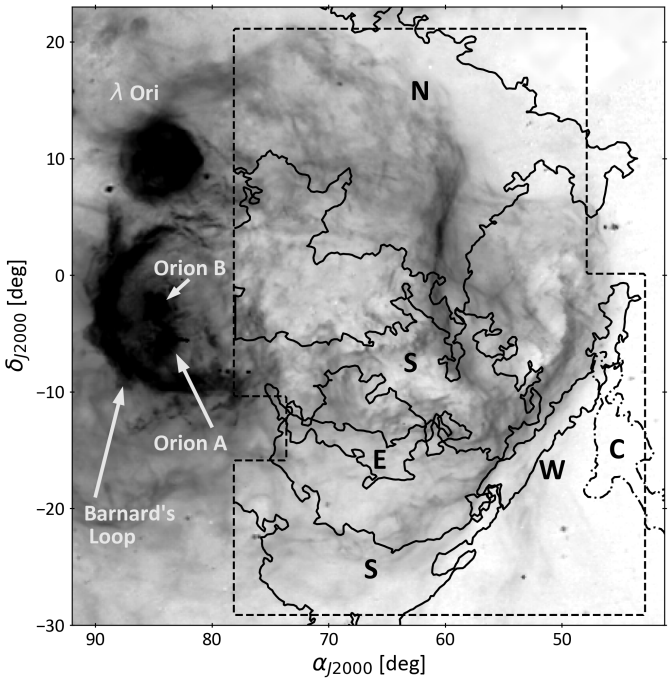

Figure 1: H_α intensity map of the Orion-Eridanus superbubble. The dashed line traces the perimeter of the analysis region. The white labels annotate key H_α features towards Orion. The black solid contours delineate the main H I shells related to the superbubble: the North Rim (N), South Loop (S), East Shell (E), and West Rim (W). The dash-dotted contour marks the Eridu cirrus (C) located outside the superbubble.

For the atomic gas, we have used the H I emission line HI4PI survey data at 16'2 resolution [10]. In order to investigate the effect of the unknown H I optical depth, we have derived all the column density $N_{\mathrm{H\,I}}$ maps for a sample of uniform spin temperatures (125, 150, 200, 300, 400, 500, 600, 700, and 800 K) and for the optically thin case. For the molecular gas, we have used the 8.′5 resolution ^{12}CO (J=1−0) observations at 115 GHz from the moment-masked CfA CO survey [4, 5]. We have completed this dataset with the CO observations of the MBM 20 cloud obtained with the Swedish-ESO Submillimetre Telescope (SEST) [17].

Warm ionised gas is visible through H_α emission. It is displayed in Fig. 1 using the composite map of the Virginia Tech Spectral line Survey (VTSS), the Southern H-Alpha Sky Survey Atlas (SHASSA), and the Wisconsin H-Alpha Mapper (WHAM) [8]. The velocity and angular resolutions are 12 km s^{-1} and 6′ (FWHM). H_α emission can, however, be efficiently absorbed by dense clouds and it does not directly trace the column density of ionised gas. We have therefore created a uniform template based on H_α emission above 14 R, in order to keep only the morphology of the main features, the normalisation being left as a free parameter in our models (see Sec. 4).

In order to trace the dust column density, we have used the optical depth at 353 GHz, τ_{353}, which has been obtained from *Planck* and *IRAS* data on the thermal emission of the large dust grains [12]. We have downgraded the map resolution from 5' to 16.2' to match the lower resolution data in our analysis.

3. Gamma-ray data

We have used ten years of Pass 8 photon data provided by the LAT between 0.25 and 63 GeV, together with the associated instrument response functions for event type P8R3_SOURCE_V2, and the corresponding isotropic spectrum for the extragalactic and residual instrumental backgrounds[1]. We have analysed the data in seven independent energy bands bounded by $10^{2.4}$, $10^{2.6}$, $10^{2.8}$, $10^{3.0}$, $10^{3.2}$, $10^{3.6}$, $10^{4.0}$, and $10^{4.8}$ MeV. The positions and spectra of the γ-ray sources in the field come from the Fermi LAT 8-year FL8Y source list[2], but we have kept their fluxes free in our models since we have analysed a longer period dataset. The GALPROP2 parameter file 54-LRYusifovXCO4z6R30-Ts150-mag2 has been used to generate an energy-dependent template of the Galactic inverse Compton (IC) emission across the analysis region [6].

3.1 Cloud distribution

Joubaud et al. have decomposed the observed H I and CO velocity spectra into a sum of individual lines with pseudo-Voigt profiles. The spatial and velocity distribution of the lines across the region, joined with distance information from dust reddening maps [9], has enabled the identification and separation of eight nearby cloud complexes that are coherent in position, velocity and distance in front of the more distant Galactic background. The contours of the main entities are displayed in Fig. 1. The structures associated with the superbubble are the North Rim, the South Loop and the East Shell, detected both in H I and CO emission lines, and the West Rim seen only in the H I data. The North Rim and West Rim trace the shell of compressed gas behind the expanding

[1] https://fermi.gsfc.nasa.gov/ssc/data/access/lat/BackgroundModels.html
[2] https://fermi.gsfc.nasa.gov/ssc/data/access/lat/fl8y/

shock. This outermost layer surrounds arcs of warm ionised gas emitting H_α lines as it recombines. The bubble interior is filled with hot X-ray emitting plasma (see Fig. 7 of [11]). The East Shell also relates to an H_α arc, but its distance and lack of X-ray shadow indicate that it is likely located inside the superbubble. Other cloud complexes seen in these directions are not related to the superbubble. The foreground MBM 20 molecular cloud lies at a distance of 120 to 180 pc between the nearest superbubble wall and the Local Bubble [18]. The nearby Eridu cirrus cloud is found just outside the West Rim at a distance of about 200 pc. Clouds behind the superbubble include the Cetus and North Taurus complexes [16], and background Galactic structures at low Galactic latitudes.

4. Model and analysis

The LAT data we have used probe cosmic rays with energies above a few GeV that uniformly permeate all gas phases up to the molecular phase seen at 115 GHz [16]. The hadronic γ-ray emission therefore traces the total gas column densities, $N_{\rm H}$, and can be modelled by a linear combination of the column densities present in the ionised, atomic, molecular, and dark neutral phases. The latter contains large amounts of gas at the H I-H_2 interface, but it is invisible in H I and CO line emission because of H I self-absorption and of the photo-dissociation and weak excitation of CO molecules in diffuse H_2. In order to trace this dark neutral medium (DNM), we have iteratively coupled γ-ray and dust analyses as dust column densities also trace the total $N_{\rm H}$ in the local ISM, albeit in a non-linear way [12, 16]. We have therefore extracted the significant γ-ray and dust residuals over the H I and CO expectations and we have used the spatial correlation between those residuals to infer the additional DNM gas column density.

4.1 Dust model

We have modelled the dust optical depth at 353 GHz in each direction as a linear combination of the gaseous contributions from the different phases (H I, DNM, CO, H II), with free y opacities to be fitted to the data, as in [14]. We have added a free isotropic term, τ_{iso}, to account for the residual noise and the uncertainty in the zero level of the dust data [13]. The $\tau_{353}(\alpha,\delta)$ model in each direction can be expressed as

$$\tau_{353}(\alpha,\delta) = \sum_{i=1}^{9} y_{\rm H\,I,}{}_i N_{\rm H\,I,}{}_i(\alpha,\delta) + \sum_{i=1}^{3} y_{\rm CO,i} W_{\rm CO,i}(\alpha,\delta) + y_{\rm DNM} N_{\rm H}^{\rm DNM}(\alpha,\delta) + \tau_{\rm H\,II} I_{\rm H\,II}(\alpha,\delta) + \tau_{iso}, \tag{4.1}$$

where $N_{\rm H\,I,}{}_i(\alpha,\delta)$, $W_{\rm CO,i}(\alpha,\delta)$, and $I_{\rm H\,II}(\alpha,\delta)$ denote the $N_{\rm H\,I}$ column density, $W_{\rm CO}$ intensity, and H II maps of the different clouds respectively. $N_{\rm H}^{\rm DNM}(\alpha,\delta)$ stands for the DNM column density deduced from the coupled γ-ray and dust analyses. The model free parameters ($y_{\rm H\,I,}{}_i$, $y_{\rm CO,i}$, $y_{\rm DNM}$, $\tau_{\rm H\,II}$ and τ_{iso}) have been fitted to the data.

4.2 Gamma-ray model

We have modelled the γ-ray emission by a linear combination of the same gaseous components as in the dust model. We have assumed that the emissivity spectrum of the gas follows the average of the local ISM, $q_{LIS}(E)$ [3], but we have left a free normalisation in each energy band to account for possible deviations in cosmic-ray density and spectrum. The model includes other

radiation components such as the Galactic IC radiation, $I_{\rm IC}(\alpha,\delta,E)$, the isotropic intensity accounting for extragalactic and instrumental backgrounds, $\mathrm{I}_{iso}(E)$, emission from the Sun and the Moon, $\mathrm{I}_{SM}(\alpha,\delta,E)$, and point sources with individual flux spectra, $S_j(E)$. The total γ-ray intensity $\mathrm{I}(\alpha,\delta,E)$, expressed in $\mathrm{cm}^{-2}\ \mathrm{s}^{-1}\ \mathrm{sr}^{-1}\ \mathrm{MeV}^{-1}$, can thus be modelled as :

$$I(\alpha,\delta,E) = q_{\rm LIS}(E) \times \left[\sum_{i=1}^{9} q_{\mathrm{H\,I},i} N_{\mathrm{H\,I},i}(\alpha,\delta) + \sum_{i=1}^{3} q_{\rm CO,i} W_{\rm CO,i}(\alpha,\delta) + q_{\rm DNM}\,\tau_{353}^{\rm DNM}(\alpha,\delta)\right] + q_{\rm iso}(E) I_{\rm iso}(E) + q_{\rm IC}(E) I_{\rm IC}(\alpha,\delta,E) + q_{\rm SM}(E) I_{\rm SM}(\alpha,\delta,E) + \sum_j q_{S_j} S_j(E)\,\delta(\alpha-\alpha_j,\delta-\delta_j),$$

with $\tau_{353}^{DNM}(\alpha,\delta)$ being the dust optical depth map resulting of the joint dust and γ-ray analyses. The model free parameters ($q_{\mathrm{H\,I},i}$, $q_{\rm CO,i}$, $q_{\rm DNM}$, $q_{\rm iso}$, $q_{\rm IC}$, $q_{\rm SM}$, q_{S_j}) have been fitted to the photon data in each energy band using a binned maximum-likelihood with Poisson statistics.

5. Results

Hadronic γ-ray emission results from the integral along the lines of sight of the cosmic-ray flux times the gas volume density, so the average γ-ray emissivity per gas nucleon in a cloud can only be inferred in the H I phase where we can directly measure the hydrogen column densities, provided corrections for self absorption. This is not possible in the other phases which require the knowledge of the CO-to-H_2 conversion factors and dust emission opacities which are known to vary with environmental conditions [16].

We present in Fig. 2 and 3 the emissivity spectra obtained in different clouds in and around the superbubble for two choices of H I spin temperatures: the 100 K value preferred by the maximum-likelihood fit and the optically thin case. The H I spin temperature has no significant impact on the shape of the emissivity spectra. The optically thin case corresponds to the minimum amount of gas possible and hence gives an upper limit to the γ-ray emissivity per gas nucleon, i.e. to the cosmic-ray flux. The results are compared with the local average emissivity, $q_{\rm LIS}$, measured in the local ISM within 500 pc from the Sun, and derived by [3] for an H I spin temperature of 140 K.

5.1 γ-ray emissivity spectra in the superbubble

We have first measured the average γ-ray emissivity in the superbubble gathering all of its clouds into a single component. The resulting average, $q_{\rm SB}$, has a similar spectral shape as $q_{\rm LIS}$, but is 6% lower with a high significance. This difference can be attributed to systematic uncertainties in the H I optical depth and is fully compatible with the $\pm$9% dispersion found in other nearby clouds for the same reason [16]. Despite its turbulent environment, the global emissivity spectrum in the superbubble is therefore consistent with the $q_{\rm LIS}$ average in the local ISM.

If we let the individual cloud parameters free, we obtain the H I γ-ray emissivity spectra shown in figure 2. The North Rim and the South Loop spectra are consistent with the superbubble average emissivity, $q_{\rm SB}$, at all energies within the uncertainties. The slightly lower emissivity found in the East Shell is not statistically significant (0.6 σ). The 8% lower emissivity in the West Rim differs from the $q_{\rm SB}$ average at a 5.6 σ confidence level. The small difference may stem from cloud to cloud variations in H I optical depth correction.

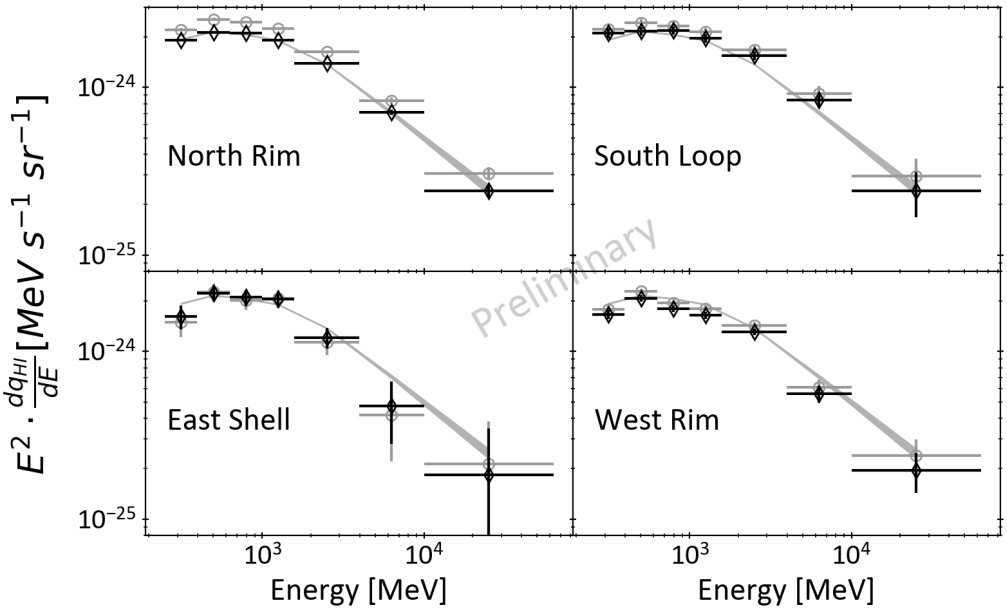

Figure 2: Spectral energy distributions of the γ-ray emissivity found per H atom in the atomic clouds of the superbubble. The data points are given for two levels of H I optical depth correction: a spin temperature $T_s = 100$ K favoured by the γ-ray fit (*black*) and the optically thin case (*grey*). The common shaded area shows the 1σ confidence region on the average emissivity, $q_{\rm SB}$, found in the superbubble for $T_s = 100$ K.

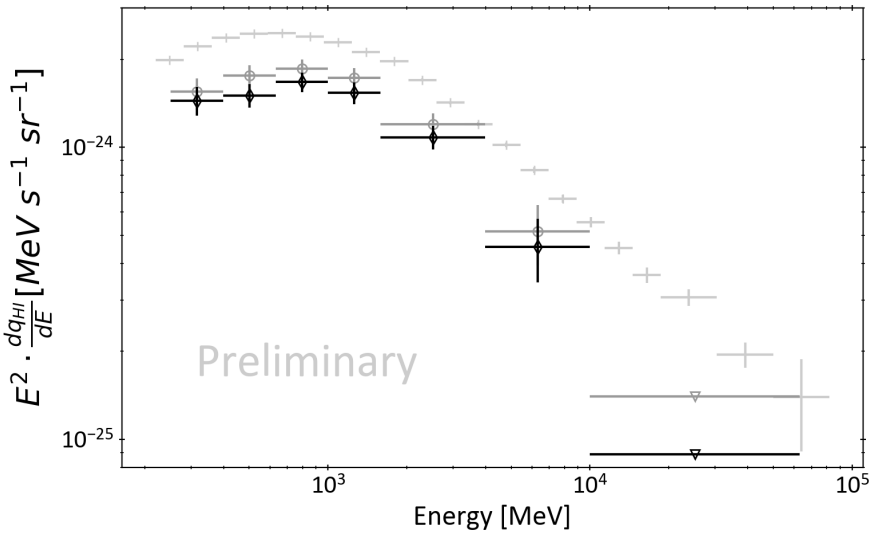

Figure 3: Spectral energy distribution of the γ-ray emissivity obtained per H atom in the Eridu cirrus. The data points are given for two levels of H I optical depth correction: a spin temperature $T_s = 100$ K favoured by the γ-ray fit (*black*) and the optically thin case (*dark grey*) which yields upper limits to the emissivity. The light grey points show the average emissivity, $q_{\rm LIS}$, found in the local ISM for $T_s = 140$ K [3].

5.2 γ-ray emissivity spectrum in the Eridu cirrus

The Eridu cirrus cloud lies outside the superbubble, at an altitude of about 200 pc below the Galactic plane. Its emissivity spectrum is displayed in Fig. 3. We find a highly significant (14 σ) drop in emissivity by 34% compared to the $q_{\rm LIS}$ spectrum characterising the rest of the local ISM. This difference cannot be attributed to H I optical depth corrections as the optically thin case gives an upper limit that is 25% below $q_{\rm LIS}$. We don't detect any DNM gas in the Eridu direction. Anyhow, adding any missing gas would imply an even smaller γ-ray emissivity per H nucleon to produce the same γ-ray photon counts. Confusion in the cloud separation in velocity is not possible as it is the only H I structure seen towards these directions. At Galactic latitudes near -50°, it is indeed too far from the Galactic plane for significant background gas contamination. Given the modest gas column densities in the cloud ($1-5\times10^{20}$ cm^{-2}), we have checked the influence of large-scale γ-ray structures from the IC and isotropic emission components. Varying those by 1σ around their best-fit spectra yields a maximum variation of 2% for the Eridu emissivity spectrum. Therefore, the spatial distribution of the gas in the Eridu cloud is significantly detected with little influence from the large-scale structures in non-gaseous γ-ray components.

6. Conclusions

All the γ-ray emissivity spectra measured in the superbubble clouds have spectral energy distributions compatible with the average found in the local ISM. The turbulent conditions of the superbubble appear to have little impact on the propagation of cosmic rays with energies between $\sim$3 and $\sim$600 GeV. We find no spectral hardening indicative of in-situ acceleration or re-acceleration of cosmic rays, even though preliminary estimates of the acceleration and spatial diffusion time scales in the superbubble suggest that re-acceleration might take place [19]. This result contrasts with the activity of the Cygnus-X superbubble where a cocoon of freshly accelerated cosmic rays has been detected [7]. Inefficient cosmic-ray acceleration in the Orion-Eridanus superbubble is puzzling given the important energy injection by massive stellar winds and past supernovae: as many as 11 supernovae should have occurred over the last 12 Myr and 62 stars with masses above 8 $M_\odot$ are still present in the Orion OB1 and λ Ori associations [20]. The Eridanus side is the older part of the superbubble, but it still contains a stream of 48 OB stars at a distance between 150 pc from the Sun and Orion [2].

Compared to the average γ-ray emissivity found in other nearby clouds, the Eridu cirrus presents a 34% loss of cosmic rays without any change in spectral energy distribution. This energy independent loss cannot be explained by cosmic-ray penetration problems in such a diffuse and low-mass cloud. A loss of this magnitude in a nearby cloud is unexpected and we are investigating if it relates to the cloud altitude off the Galactic plane and/or to its orientation with respect to magnetic field lines in the Galactic halo.

Acknowledgments

We acknowledge support from the ANR-DFG grant CRiBs (ANR-15-CE31-0019-01) for this work. The *Fermi*-LAT Collaboration acknowledges support for LAT development, operation and data analysis from NASA and DOE (United States), CEA/Irfu and IN2P3/CNRS (France), ASI and INFN (Italy), MEXT, KEK, and JAXA (Japan), and the K.A. Wallenberg Foundation, the Swedish Research Council and the National Space Board (Sweden). Science analysis support in the operations phase from INAF (Italy) and

CNES (France) is also gratefully acknowledged. This work performed in part under DOE Contract DE-AC02-76SF00515.

References

[1] J. Bally. *Overview of the Orion Complex*, volume 4, page 459. 2008. [arXiv:0812.0046]

[2] H. Bouy and J. Alves. *Cosmography of OB stars in the solar neighbourhood*. *A&A*, 584:A26, 2015.

[3] J.-M. Casandjian. *Local* H I *emissivity measured with Fermi LAT and implications for cosmic-ray spectra*. *ApJ.*, 806:240, 2015. [arXiv:1506.00047]

[4] T. M. Dame, Dap Hartmann, and P. Thaddeus. *The Milky Way in Molecular Clouds: A New Complete CO Survey*. *ApJ.*, 547:792, 2001. [astro-ph/0009217]

[5] T. M. Dame and P. Thaddeus. *A Large Extension of the CfA Galactic CO Survey*. *Astronomical Society of the Pacific Conference Series*, 317:66, 2004. [astro-ph/0310102]

[6] Fermi-LAT Collaboration, et al. *Fermi-LAT Observations of the Diffuse γ-Ray Emission: Implications for Cosmic Rays and the Interstellar Medium*. *ApJ.*, 750:3, 2012. [arXiv:1202.4039]

[7] Fermi-LAT collaboration, et al. *A Cocoon of Freshly Accelerated Cosmic Rays Detected by Fermi in the Cygnus Superbubble*. *Science*, 334:1103, 2011.

[8] D. P. Finkbeiner. *A Full-Sky Hα Template for Microwave Foreground Prediction*. *ApJ. Suppl.*, 146:407, 2003. [astro-ph/0301558]

[9] G. M. Green, et al. *Galactic reddening in 3D from stellar photometry - an improved map*. *MNRAS*, 478:651, 2018. [arXiv:1801.03555]

[10] HI4PI Collaboration, et al. *HI4PI: A full-sky HI survey based on EBHIS and GASS*. *A&A*, 594:A116, 2016. [arXiv:1610.06175]

[11] T. Joubaud, I. A. Grenier, J. Ballet, and Soler J. D. *Gas shells and magnetic fields in the Orion-Eridanus superbubble*. *A&A*, submitted, 2019.

[12] Planck Collaboration, et al. *Planck intermediate results. XVII. Emission of dust in the diffuse interstellar medium from the far-infrared to microwave frequencies*. *A&A*, 566:A55, 2014. [arXiv:1312.5446]

[13] Planck Collaboration, et al. *Planck 2013 results. XI. All-sky model of thermal dust emission*. *A&A*, 571:A11, 2014. [1312.1300]

[14] Planck Collaboration, Fermi Collaboration, et al. *Planck intermediate results. XXVIII. Interstellar gas and dust in the Chamaeleon clouds as seen by Fermi LAT and Planck*. *A&A*, 582:A31, 2015. [arXiv:1409.3268]

[15] A. Pon, B. B. Ochsendorf, J. Alves, et al. *Kompaneets Model Fitting of the Orion-Eridanus Superbubble. II. Thinking Outside of Barnard's Loop*. *ApJ.*, 827:42, 2016. [arXiv:1606.02296]

[16] Q. Remy, I. A. Grenier, D. J. Marshall, and J. M. Casandjian. *Cosmic rays, gas and dust in nearby anticentre clouds. I. CO-to-H_2 conversion factors and dust opacities*. *A&A*, 601:A78, 2017. [arXiv:1703.05237]

[17] D. Russeil, M. Juvela, K. Lehtinen, et al. *Morphology and kinematics of Lynds 1642. Multivariate analysis of CO maps of a translucent cloud*. *A&A*, 409:135, 2003. [astro-ph/0309275]

[18] E. F. Schlafly, et al. *A Large Catalog of Accurate Distances to Molecular Clouds from PS1 Photometry*. *ApJ.*, 786:29, 2014. [arXiv:1403.3393]

[19] T. Tolksdorf, I. A. Grenier, T. Joubaud, and R. Schlickeiser. *Cosmic rays in superbubbles*. *ApJ.*, 879:66, 2019.

[20] R. Voss, R. Diehl, J. S. Vink, and D. H. Hartmann. *Probing the evolving massive star population in Orion with kinematic and radioactive tracers*. *A&A*, 520:A51, 2010. [arXiv:1005.3827]